Int J Adv Manuf Technol (2015) 79:729–738
DOI 10.1007/s00170-015-6870-3

ORIGINAL ARTICLE

A new test part to identify performance of five-axis machine tool—part I: geometrical and kinematic characteristics of S part

Wei Wang · Zhong Jiang · Wenjian Tao · Wenhao Zhuang

Received: 3 June 2014 / Accepted: 1 December 2014 / Published online: 18 February 2015

Abstract The manufacturing test part applications are essential for representations of machines' capabilities. Commonly used NAS979 has been known to insufficiently evaluate the combination motions of rotary axes. Thus, a new test part, S part, has been presented to satisfy the increasing demand of a five-axis machine. In this paper, the model of S part is described in detail, which presents more characteristics in three-dimensional surface contours. According to the kinematics analysis, the speed of each axis and feed rate falls down and rises up on several positions. Each axis reverses the motion during the machining. Therefore, the S part makes high requirement on machine's dynamic response.

Keywords Test part · Complex surface · Dynamic performance · CNC machine

1 Introduction

Five-axis machines are extensively used in complicated surface machining, especially for the high-speed machine with higher metal removal rate, significantly shorten cutting time, and improved surface quality. In the highly competitive market, machine tool manufacturers build high-precision machines, while at the same time keeping price as low as possible. The history of machine tools is the history of the precision of machine tool. According to the references [1], there are four types of error sources that mainly influence the accuracy of the machining, which are categorized as geometric error, control system error, thermal error, and deformation under cutting forces. Geometric error comes from the structural imperfections or assembly errors on joints, such as misalignments of axes and slideway degradation. Today, in a five-axis machine tool, geometric accuracy has been significantly improved over that of a conventional three-axis machine. The left three errors which came from dynamic machining process, called dynamic errors, have been the significant contributors to the part of dimensional errors [2]. However, as a standard, describing the inspection of motion accuracy of a five-axis machine tool, ISO only defines measurement schemes to evaluate some limit dynamic errors, such as accuracy of position and repeatability of position. For a five-axis machine configuration having a tilting rotary table, ISO 230 develops measurement scheme of kinematics errors of rotary axes [3]. Besides these, there is a lack of standard measurement methods on other dynamic errors. Thus, many researchers use the new instruments, such as double ball bare or R test to identify these errors [4, 5]. However, such tests can only be applied in a fixed trace. It is hard to simulate the processing of complex surface and cannot move as real feed rate. More importantly, these dynamic errors are measured in no-load condition. Typically, machine tool users are more concerned with the accuracy of a five-axis machine when it performs actual machining. The precision of the machine tool determines the machining precision of parts. Therefore, the acceptance of part precision is a key section in the acceptance of a machine tool. So far, the best known test part for five-axis machine is NAS979 [6]. The geometry of NAS979 is a cone frustum with a 15° rotary angle along a horizontal plane. Once a NAS979 part is machined, the results are used to define a series of measurements,

W. Wang (✉) · Z. Jiang · W. Tao · W. Zhuang
School of Mechatronics Engineering, University of Electronic Science and Technology of China, Chengdu 611731, China
e-mail: wangwhit@163.com

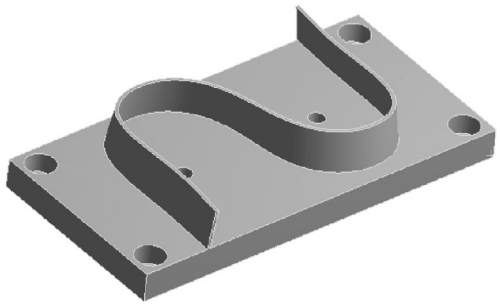

Fig. 1 3D view of S part

such as square, parallelism, and circularity. NAS979 was created in 1969 and then developed as a basis of the standard in ISO 10791-7 [7]. But it is hardly used to evaluate the coupled motion between two rotary axes or the combination of linear-rotary axes. Nowadays, many users demand high precision in three-dimensional (3D) contouring application for a five-axis machine [8]. A five-axis machine tool qualified by NAS979 often has other machining problems such as unsmooth profile or poor surface quality. Since the demand for a five-axis machine is increasing rapidly, there is still the lack of test part or validation tests [9].

That is why we need new test parts to testify a five-axis machine's performance. A new S-shaped test part, called S part, has been presented to demonstrate the machine tool's capabilities [10]. It has made some successful applications in many fairs or showrooms. This paper gives the detailed introduction of S parts and characteristics of S part. It can explain why the S part is so special for five-axis machine tool. The validation of S part to evaluate the performance of five-axis machine and some experiments will be furthermore discussed in part II.

2 Modeling of S part

2.1 Description on S part

Figure 1 is a 3D view of S part. The shape of S part looks like letter "S," but it is real different. Projected S part in a horizontal plane, the up and down boundary spline curves do not parallel and cross at point *P*, seen in the engineering drawings of Fig. 2.

2.2 Modeling process

The process of S part modeling is as follows. First, construct the boundary curve of S part, which is a three-order uniform rational B-spline curve. The equation of B-spline curve is expressed in Eq. (1). Here, $P_i(i=0,1,L,n)$ are the control points which affect the shape of curve. $N_{i,m}(u)$ is the base function, m is the order of spline curve.

$$Q(u) = \sum_{i=0}^{n} P_i N_{i,m}(u) \tag{1}$$

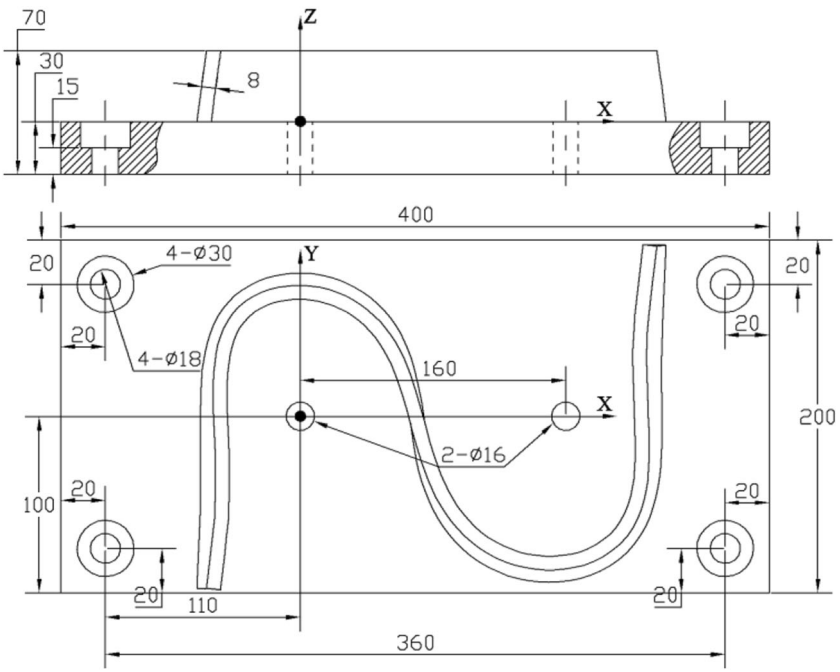

Fig. 2 Engineering drawings of S part

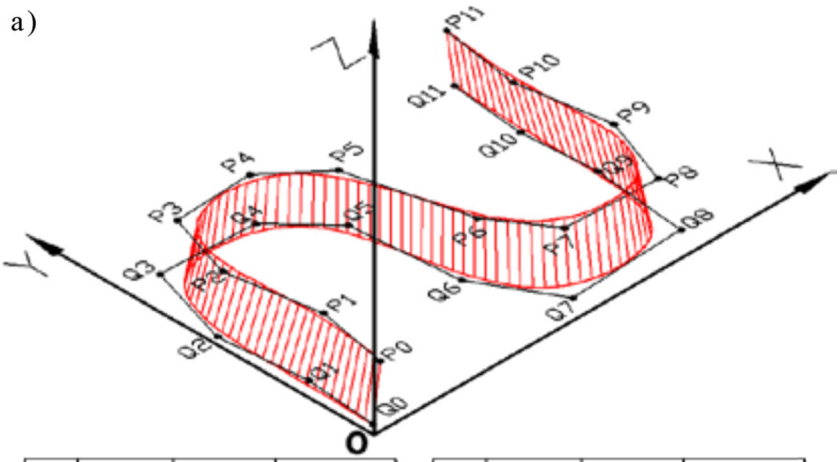

Pi	POS_X	POS_Y	POS_Z
P0	12	2.5	40
P1	21	57	40
P2	12	121	40
P3	27	176	40
P4	92	175	40
P5	123	142	40
P6	142	67	40
P7	170	18	40
P8	246	17	40
P9	259	85	40
P10	250	141	40
P11	258	197.5	40

Qi	POS_X	POS_Y	POS_Z
Q0	6	2.5	0
Q1	9	57	0
Q2	5	121	0
Q3	25	185	0
Q4	95	182	0
Q5	130	145	0
Q6	137	65	0
Q7	168	10	0
Q8	255	14	0
Q9	262	85	0
Q10	261	141	0
Q11	264	197.5	0

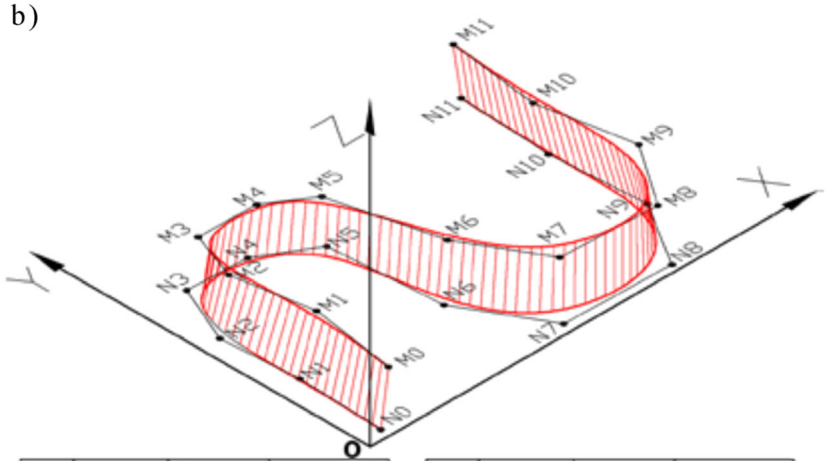

Mi	POS_X	POS_Y	POS_Z
M0	22	2.5	40
M1	32	69	40
M2	22	128	40
M3	36	166	40
M4	81	165	40
M5	112	145	40
M6	132	66	40
M7	164	10	40
M8	238	7	40
M9	272	56	40
M10	259	126	40
P11	268	197.5	40

Ni	POS_X	POS_Y	POS_Z
N0	16	2.5	0
N1	19	69	0
N2	15	128	0
N3	35	174	0
N4	81	172	0
N5	120	149	0
N6	126	63	0
N7	160	3	0
N8	243	1	0
N9	275	52	0
N10	270	125	0
N11	274	197.5	0

Fig. 3 **a** Inner surface of S part. **b** Outer surface of S part

The base function got by De Boor-Cox method [11]. Each segment is composed of four control points and has four base functions. The base functions on the first two segments and the last two segments are different.

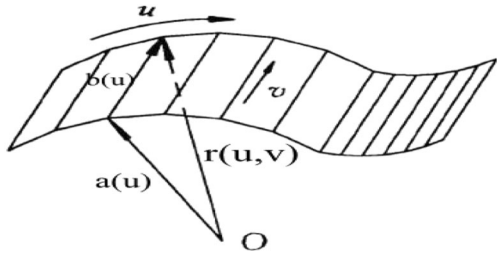

Fig. 4 The mathematic model of S surface

The other segments have the same one. They are expressed as follows:

At first segment,

$$\begin{cases} N_{1,3}(u) = -u^3 + 3u^2 - 3u + 1 \\ N_{2,3}(u) = \frac{7}{4}u^3 - \frac{9}{2}u^2 + 3u \\ N_{3,3}(u) = -\frac{11}{12}u^3 + \frac{3}{2}u^2 \\ N_{4,3}(u) = \frac{1}{6}u^3 \end{cases} \tag{2}$$

The second segment,

$$\begin{cases} N_{1,3}(u) = -\frac{1}{4}\left(u^3 + 3u^2 - 3u + 1\right) \\ N_{2,3}(u) = \frac{1}{12}\left(7u^3 - 15u^2 + 3u + 7\right) \\ N_{3,3}(u) = -\frac{1}{6}\left(3u^3 - 3u^2 - 3u + 1\right) \\ N_{4,3}(u) = \frac{1}{6}u^3 \end{cases} \tag{3}$$

The third to $n-1$ segment,

$$\begin{cases} N_{1,3}(u) = \frac{1}{6}(1-u)^3 \\ N_{2,3}(u) = \frac{1}{6}\left(3u^3 - 6u^2 + 4\right) \\ N_{3,3}(u) = \frac{1}{6}\left(-3u^3 + 3u^2 + 3u + 1\right) \\ N_{4,3}(u) = \frac{1}{6}u^3 \end{cases} \tag{4}$$

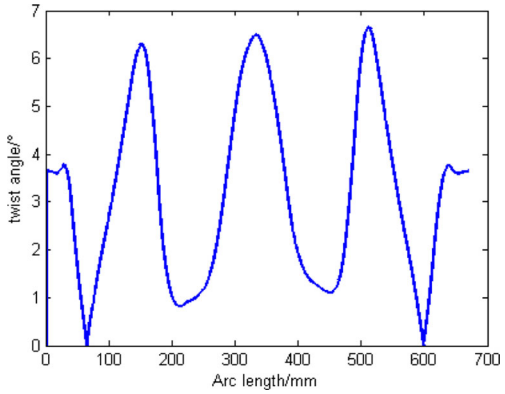

Fig. 6 Distribution of twist angle on S part

The last but one segment,

$$\begin{cases} N_{1,3}(u) = -\frac{1}{6}\left(u^3 - 3u^2 + 3u - 1\right) \\ N_{2,3}(u) = \frac{1}{2}u^3 - u^2 + \frac{2}{3} \\ N_{3,3}(u) = -\frac{1}{12}\left(7u^3 - 6u^2 - 6u - 2\right) \\ N_{4,3}(u) = \frac{1}{4}u^3 \end{cases} \tag{5}$$

The last segment,

$$\begin{cases} N_{1,3}(u) = -\frac{1}{6}\left(u^3 - 3u^2 + 3u - 1\right) \\ N_{2,3}(u) = \frac{1}{12}\left(11u^3 - 15u^2 - 3u + 7\right) \\ N_{3,3}(u) = -\frac{1}{4}\left(7u^3 - 3u^2 - 3u - 1\right) \\ N_{4,3}(u) = u^3 \end{cases} \tag{6}$$

Two sets of control points P_i and Q_i are given in Fig. 3. Thus, two boundary B-spline curves are created by these sets of points. The inner surface of S part is composed by sweeping the bus bar along the boundary curves.

Second, another two sets of points M_i and N_i are shown in Fig. 3b. Similarly, the outer surface of S part is composed. Finally, construct two ruler surfaces into S part.

Fig. 5 Twist angle defining

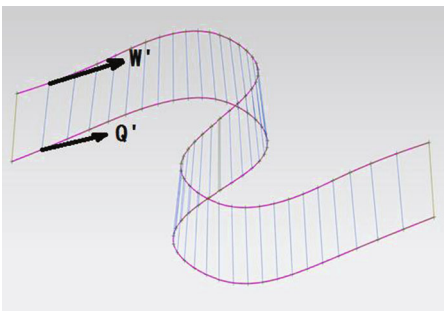

a)

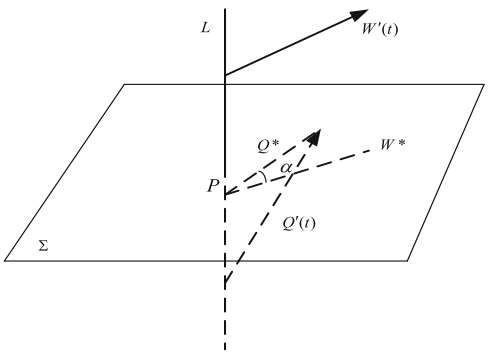

b)

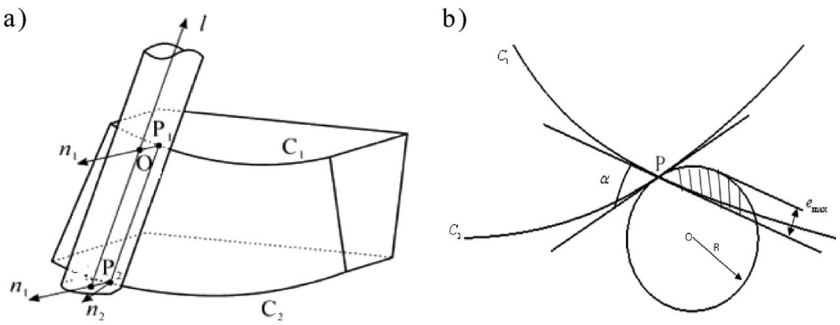

Fig. 7 **a** Milling process at one point of S part. **b** Projection of milling process

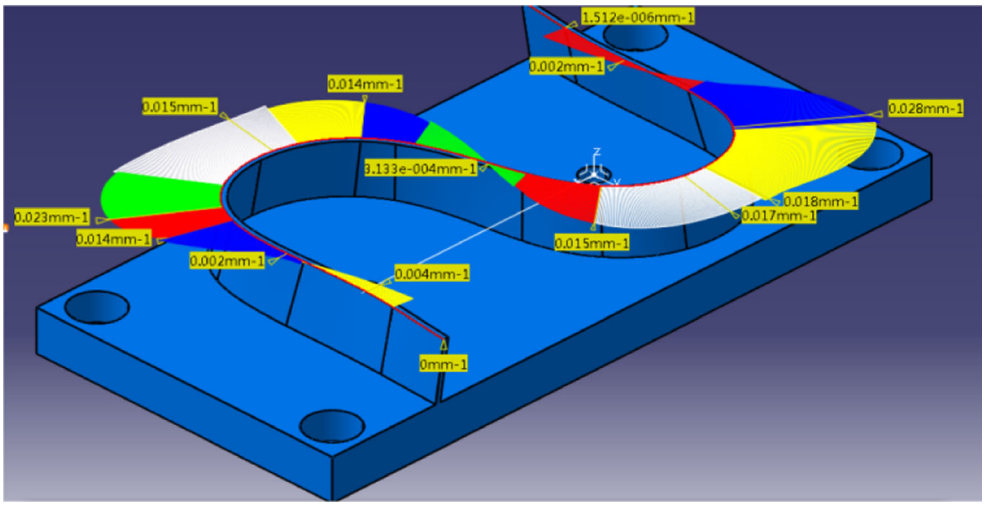

Fig. 8 Variable curvature on upper boundary line

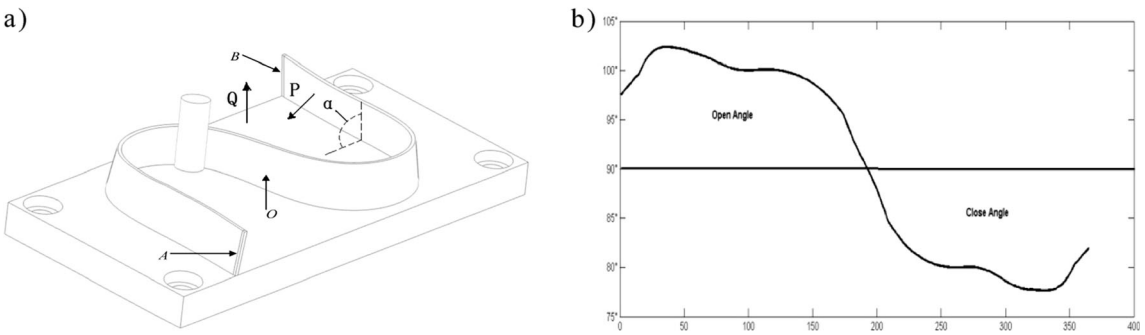

Fig. 9 **a** Machining angle defining. **b** Distribution of include angle during machining

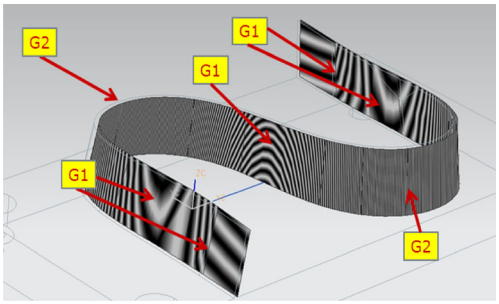

Fig. 10 S surface continuity

3 Geometric characteristic of S part

3.1 Non-developed rule surface

The mathematic model of surface can be described in Eq. (7). Here, μ is the parameter along the boundary curves, v is the parameter along a bus bar. The normal line of S surface can be gotten by multiplication cross its partial derivative in Eq. (8). As can be seen, v is variable on the same bus bar. So the normal line on the same bus bar is not parallel. Thus, S surface is a non-developable ruled surface (Fig. 4).

$$\vec{r} = \vec{a}(\mu) + \vec{v}\,\vec{b}(\mu) \tag{7}$$

$$\begin{aligned}\vec{r}_u \times \vec{r}_v &= \left(\vec{a}'(u) + v\vec{b}'(u)\right) \times \vec{b}(u) \\ &= \vec{a}'(u) \times \vec{b}(u) + v\vec{b}'(u) \times \vec{b}(u)\end{aligned} \tag{8}$$

As a non-developable surface, it cannot be put in a horizontal plane. Therefore, two boundary curves will have the twist angle in the normal plane of the bus bar. As seen in Fig. 5a, $W'(t)$ and $Q'(t)$ are tangent lines of two boundary curves of S part. They are in the same bar L. As seen in Fig. 5b, P is any point in bus bar L. There is a normal plane Σ through point P and perpendicular to the bus bar L. W^* and Q^* are projection of tangent lines in normal plane Σ. The twist angle α is defined as the intersection angle of W^* and Q^* expressed as

$$\cos\alpha = \frac{W^* \cdot Q^*}{|W^*||Q^*|} \tag{9}$$

Figure 6 shows the distribution of twist angle on S part at the points of bottom boundary curve. On the whole surface, the twist angle rises up and down with several peaks. The maximum value is about seven angular degrees at cross point of two boundary lines. Due to the existence of twist angle, S part can only be processed in a five-axis machine with the tool axis orientation along the variable bus bar direction. On the other hand, there are the principle errors during the milling process. As seen in Fig. 7a, C_1 and C_2 are two boundary curves of S part. P_1 and P_2 are points at the curves. n_1 and n_2 are normal vectors of S surface at point P_1 and P_2. l is the tool axis orientation. Obviously with the twist angle, n_2 is not equal to n_1. Seen in Fig. 6b, two boundary curves are projected into the normal plane of bus bar. Regarding the feed direction along the tangent line of C_1 or C_2, the shadow area is the principle error, which can be expressed as

$$e(\alpha) = R + R_2 - \sqrt{R^2 + {R_2}^2 + 2RR_2\cos\alpha} \tag{10}$$

Here, R is the radius of milling tool, α is the twist angle, R_2 is the curvature of curve C_2 at point P_2. So the maximum principle error appears at the maximum twist angle, which is about 8 μm. In many complex surfaces such as blade, aircraft wings are modeling with the twist angle, so it is necessary to keep the twist angle on S part. For reducing the principle error on S part, S part can be machined with several milling layers. Then the twist angle α will be smaller by calculating between boundary curves C_1 and C_2. It will, on the other hand, fully present the performance of machine center and require the high accuracy of rotary movement.

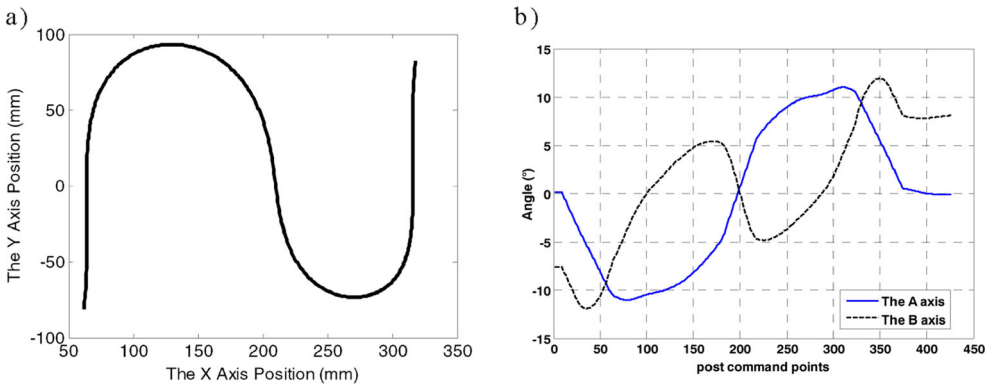

Fig. 11 **a** Commands of X, Y axis. **b** Commands of A, B axes

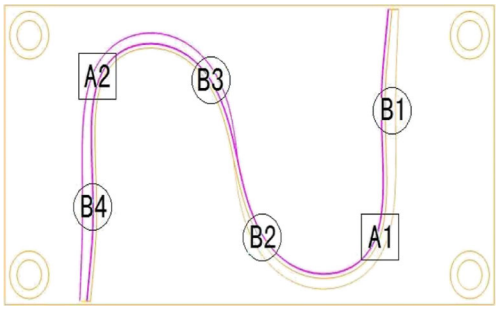

Fig. 12 Reserving motion for *A*, *B* axes

3.2 Variable curvature

Suppose that the curve $L{:}u{=}u(t)$, $v{=}v(t)$ is the any curve through the point $P_0(u_0,v_0)$ on S part, the equation of curve L can be derived as

$$\boldsymbol{r} = \boldsymbol{r}(u(t), v(t)) \tag{11}$$

So the tangent line of curve L at point P_0 is

$$r'\Big|_{t_0} = \boldsymbol{r}_u(u_0, v_0)\left(\frac{du}{dt}\right)\Big|_{t_0} + \boldsymbol{r}_v(u_0, v_0)\left(\frac{dv}{dt}\right)\Big|_{t_0} \tag{12}$$

The curvature of curve L at point P_0 is written as

$$k = \frac{|r' \times r''|}{|r'|^3} \tag{13}$$

Figure 8 shows different curvatures in the up boundary curve. At the beginning, the curvature is very small similar to the straight line. Then the curvature changes its bending direction and quickly increases. After passing the maximum circle, the curvature gradually decreases. Subsequently, the curvature reverses the bending direction again at the cross point of two boundary projection curves. The curvature plot at the right side is the mirror symmetry through cross point. With so many different circles pieced together, S part can show the machining performances as a complex surface with rapid change of curvature.

3.3 Open angle and close angle

Seen in Fig. 9a, $\boldsymbol{P}$ is the normal line of S surface, $\boldsymbol{Q}$ is the normal line of the horizontal plane. In S surface, the tangent vector $\overrightarrow{r}_u$, $\overrightarrow{r}_v$ and the point P_0 can define the tangent plane of S part at point P_0.So the normal vector of S surface can be known as

$$P(u_0, v_0) = \frac{\boldsymbol{r}_u(u_0, v_0) \times \boldsymbol{r}_v(u_0, v_0)}{|\boldsymbol{r}_u(u_0, v_0) \times \boldsymbol{r}_v(u_0, v_0)|} \tag{14}$$

The normal vector of horizontal plan $\boldsymbol{J}$ at the foundation bed of S part is

$$Q = (a, b, c) \tag{15}$$

Here, $a^2{+}b^2{+}c^2{=}1$. The intersection angle between vector $\boldsymbol{I}$ and $\boldsymbol{J}$ is

$$\cos\gamma = \frac{P \cdot Q}{|P| \times |Q|} \tag{16}$$

Here, the angle γ between $\boldsymbol{P}$ and $\boldsymbol{Q}$ presents the tool axis orientation during the milling process. In the outer surface of S part, between the area A and O, γ is less than 90°, which is called close angle of the tool. Between the areas O and B, γ is more than 90°, which is called open angle of the tool. The changes of machining angle during the process are shown in Fig. 9b. At the middle point of the boundary curve, the tool vector transfers from one quadrant to another quadrant. Therefore, S part can show the performance of the machine tool in all directions.

3.4 Discontinuity on S surface

The boundary curve of S part is a three-order B-spline curve, which means the curve has two order continuity, geometric continuity, tangent continuity, and curvature continuity. However, it does not mean the surface has the corresponding

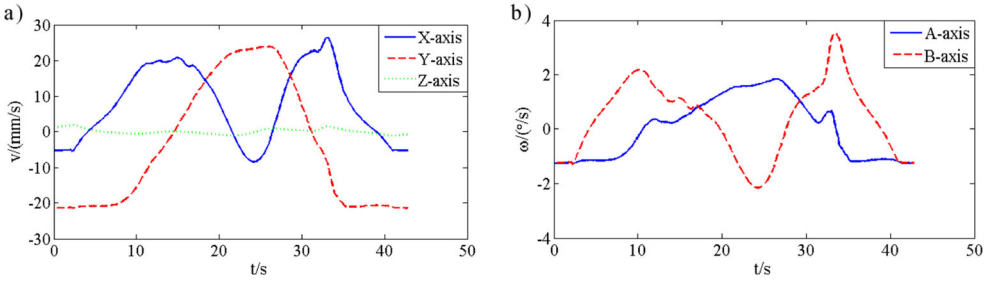

Fig. 13 **a** Translation axis ideal velocity. **b** Rotary axis ideal velocity

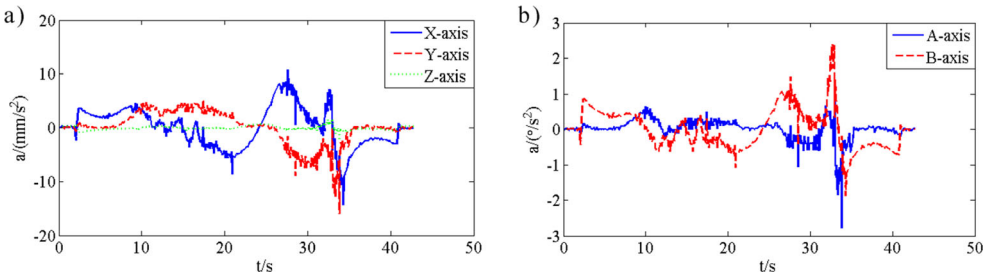

Fig. 14 **a** Translation axis ideal acceleration. **b** Rotary axis acceleration

continuity, which needs to satisfy the continuity along every possible curve. Usually, the normal curvatures of the surface are calculated to show the changes at different directions. As said above, the mathematic model of S part surface is expressed in Eq. (7) as

$$\vec{r} = \vec{a}(\mu) + \vec{v}\,\vec{b}(\mu)$$

Two principle curvatures of the surface k_1,k_2 can be calculated as

$$\left(EG-F^2\right)k^2 + (EN-2FM+GL)k + \left(LN-M^2\right) = 0 \quad (17)$$

Here, E, F, G, L, M, N are respectively fundamental quantities of first and second kind for surfaces, which are known as

$$\begin{cases} E = r_u{}^2 = (a' + vb')^2 \\ F = r_u r_v = (a' + vb')b \\ G = r_v{}^2 = b^2 \\ L = nr_{uu} = \dfrac{a' \times b + vb' \times b}{\sqrt{EG-F^2}}[a'' + vb''] \\ M = nr_{uv} = \dfrac{(a' \times b)\cdot b'}{\sqrt{EG-F^2}} = \dfrac{(a', b, b')}{\sqrt{EG-F^2}} \\ N = r_{vv} n = 0 \end{cases} \quad (18)$$

The directions of two principle curvatures du:dv are calculated as

$$(EM-FL)du^2 + (EN-GL)dudv + (FN-GM)dv^2 = 0 \quad (19)$$

Then, the normal curvatures of the surface k_n can be expressed as

$$k_n = k_1\cos^2\varphi + k_2\sin^2\varphi \quad (20)$$

Here, φ is the included angle between the principle direction and any tangent direction. Substituting the include angle from 0 to 2 π, the normal curvature along different curves are known. Another way to find out the continuous area is using a light. Choosing a light projected on S part surface, the strips on the surface could show the continuity. If the strips change the shape or jump sideway as they cross the connection, this indicates geometric continuity G0 at the surface. If the stripes cross the connection but turn sharply, this means tangent continuity G1. If the stripes match and continuous smoothly over the connection, this means curvature continuity G2. As seen in Fig. 10, the strips at the first and last area turn sharply, which satisfy G1 continuity. The most of area on S part has the same finest strips, which satisfy G2 continuity. When the machine tool crosses these connection areas, the discontinuity could give rise to the vibration or impact. It may lead to the poor surface quality. In the other words, it requires the high dynamic performance of the machine tool.

4 Kinematic characteristic of S part

4.1 The tool position on S path

Input S part model into CAM software such as UG, VERI CUT. Select one type of machine tool, then the position of tool can be derived. Here, take a type of machine tool with two rotary axes A, B as an example. The coordinate of the tool center are plotted in Fig. 11a, which are similar to the projection of S part in XOY plane only without considering the radius of the tool. The Z-axis does not have too much displacement on each layer milling. So it does not show in the figure. For the tool axis orientation, the commands of A, B axes are shown in Fig. 11b. As can be seen, the motions of each axis do

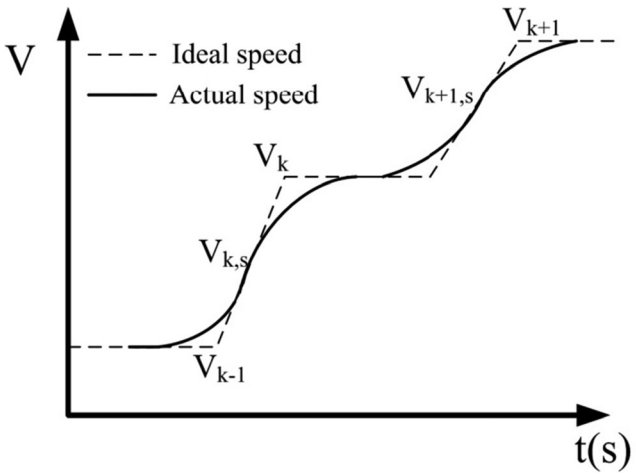

Fig. 15 S-shaped acceleration model

Table 1 Maximum speed, acceleration and jerk of five axes

	X	*Y*	*Z*	*A*	*B*
V_{max}	15 m/min	15 m/min	15 m/min	15 r/min	15 r/min
A_{max}	0.5 m/s^2	0.5 m/s^2	0.5 m/s^2	0.5 r/s^2	0.5 r/s^2
J_{max}	10 m/s^3	10 m/s^3	10 m/s^3	10 r/s^3	10 r/s^3

not change in a linear relationship. Thus, all axes will not have a constant speed during the machining. Furthermore, each axis reserves the direction for several times, such as three times for *A*-axis and four times for *B*-axis seen in Fig. 12. The gaps in rotary axis will present strong effect on dynamic errors.

4.2 Ideal speed of five axes

When the tool moves from one point $P_1(X_1, Y_1, Z_1, A_1, B_1)$ to another point $P_2(X_2, Y_2, Z_2, A_2, B_2)$, the feed rate is set as *V*. On a very short time, the feed rate can be considered as a constant. So the moving time ΔT_1 is

$$\Delta T_1 = (P_2 - P_1) \Big/ V \tag{21}$$

During the process, five axes coupled moves and have the same moving time. On a short moving time, the axis speed can also be expected to be constant. Thus, the ideal speed of each axis can be derived by the displacement dividing the time,

$$\begin{cases} V_{x1} = (X_2 - X_1) \Big/ \Delta T_1 \\ V_{y1} = (Y_2 - Y_1) \Big/ \Delta T_1 \\ V_{z1} = (Z_2 - Z_1) \Big/ \Delta T_1 \\ V_{A1} = (A_2 - A_1) \Big/ \Delta T_1 \\ V_{B1} = (B_2 - B_1) \Big/ \Delta T_1 \end{cases} \tag{22}$$

Given that the feed rate is 900 mm/min, the ideal speed of each axis is shown in Fig. 13. The ideal acceleration can also be derived by the difference of speed dividing the moving time again in Fig. 14. All axes have an obvious fluctuation on speed and acceleration except the *Z*-axis. It requires the machine has a good ability on acceleration and deceleration to get through S part. Especially for the latter half of the process, the axes of *A*, *B*, *X*, and *Y* have a very high acceleration and deceleration. Such movements could lead to the violent impact forces. It is well known that the stiffness of the axis is very important on the high-speed motion. Therefore, S part tests the ability of anti-vibration on each axis especially for the rotary axes.

4.3 Actual speed of five axes

As said above, the speed and acceleration of each axis fluctuate much and endure a lot of impact. In avoiding such violent impacts, usually the machine tool will set a limit on the acceleration and jerk. If does so, it would make the change of speed smoothly to avoid the sudden load. Before meeting the larger acceleration or jerk, the digital control system of the machine center will also choose to speed up in advance [12]. As seen in Fig. 15, usually the speed of axis chooses S-shaped acceleration or deceleration to keep the traces of speed moving smoothly [13]. However, if some positions still have a higher acceleration that is over the maximum limit of design requirement, at this time, the digital control system will cut the peaks and keep the actual acceleration as the limit to avoid greater impact. So does for the jerk. During the calculation, the actual jerk could change firstly seen in Eq. (23), then for the acceleration in Eq. (24), and next for the speed in Eq. (25).

$$J(t) = \begin{cases} J_{max} & t_0 < t < t_1 \\ -J_{max} & t_1 < t < t_2 \end{cases} \tag{23}$$

$$a(t) = \begin{cases} J_{max} \cdot t & t_0 < t < t_1 \\ J_{max} \cdot (t_1 - t_0) - J_{max} \cdot (t - t_1) & t_1 < t < t_2 \end{cases} \tag{24}$$

$$v(t) = \begin{cases} v_0 + J_{max} \cdot \dfrac{(t-t_0)^2}{2} & t_0 < t < t_1 \\ v_1 + A_1(t - t_1) - J_{max} \cdot \dfrac{(t-t_1)^2}{2} & t_1 < t < t_2 \end{cases} \tag{25}$$

Table 1 shows a case of maximum of speed, acceleration, and jerk. Through the equations listed above, the actual speed and acceleration of five axes are shown in Figs. 16 and 17. As can be seen, the maximum speed and acceleration has decreased compared with ideal one. So the running time correspondingly increases. The actual speed and acceleration have

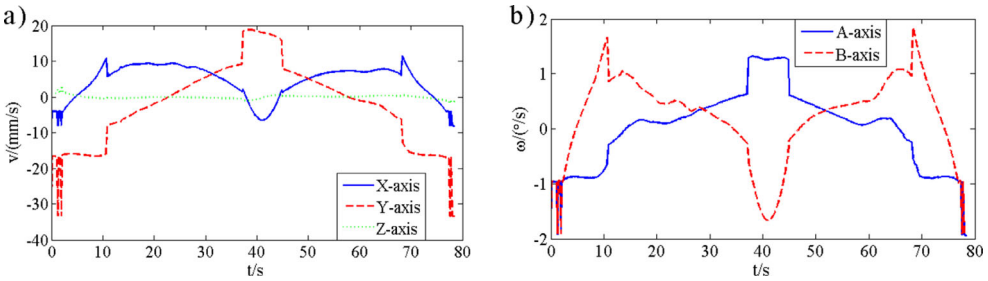

Fig. 16 **a** Actual speed of linear axis. **b** Actual speed of rotary axis

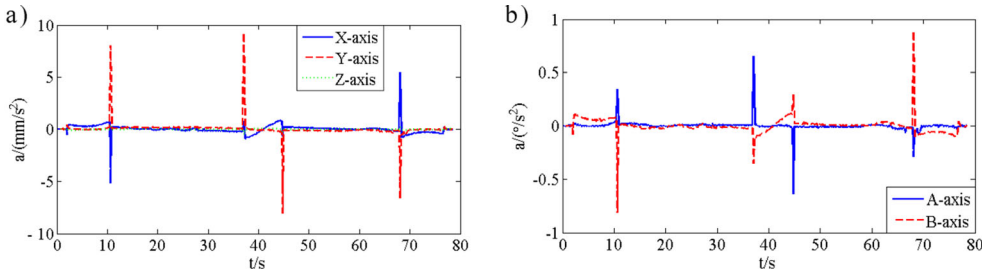

Fig. 17 **a** Actual acceleration of linear axis. **b** Actual acceleration of rotary axis

the same trend with the ideal one, but the time occurred at maximum or minimum speed or acceleration has been delayed for a while. Compose the speeds of five axes together, the actual feed rate can be derived in Fig. 18. Obviously, the actual feed rate does not keep constant as the ideal one. The trend of feed rate seems to correspond to the change of acceleration and has some relationship with the curvature of S part. Therefore, the machine center to get through S part should have the ability of quick response, anti-impact, and anti-vibration. On the other hand, S part will easily show the poor surface quality if the machine center does not have a good dynamic performance.

5 Conclusion

As a five-axis machine center has been more widely accepted, it is critical to know the performance of machine center. Here, a new test part, S part, is presented to be well understood and strategies for either avoidance or compensation of precision loss of a five-axis machine center. S part is developed by a set of given discrete control points as a non-developable rule surface, which presents more geometric characteristics on three dimensional surface contours. S part has a variable twist angle and its boundary curves have a different curvature. For this reason, it can only be machined by a five-axis machine tool. During the process, the position of the tool changes in a wide range from close angle to open angle. In the whole surface, S part does not have uniform continuity. From kinematics analysis, the motions of each axis change nonlinearly and reverse the direction in several positions. The speed and acceleration of each axis quickly falls down and increases up. Such movements lead to the impact, which tests quickly response and anti-vibration of machine tool. The performance of the machine, especially for the rotary axes, has been fully shown in S part. The validation of S part and cutting experiment will be further discussed in part II.

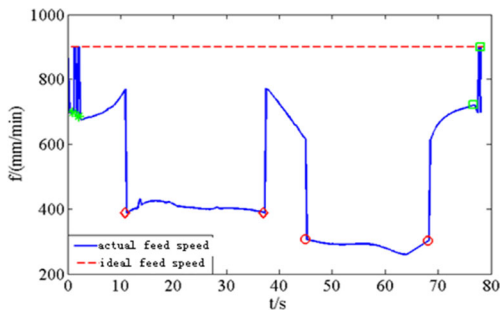

Fig. 18 Composed actual feed rate

Acknowledgments This work is supported by National Science and Foundation of China (51205048) and Open Research Foundation of State Key Lab. of Digital Manufacturing Equipment and Technology in Huazhong University of Science and Technology (DMETKF2012006)

References

1. Schmitz TL, Ziegert JC, Zapata R (2006) Part accuracy in high-speed machining: preliminary results. Proceeding of MESC, Ypsilanti, USA, MSEC:851–858
2. Andolfatto LL, Mayer JRR (2011) Evaluation of servo, geometric and dynamic error sources on five-axis high-speed machine tool. Int J Mach Tools Manuf 51:787–796
3. ISO 230–1 (1996) Test code for machine tools—part 1: geometric accuracy of machines operating under no-load or finishing conditions
4. Ibaraki S, Oyama C, Otsubo H (2011) Construction of an error map of rotary axes on a five-axis machining center by static R-test. Int J Mach Tools Manuf 51:190–200
5. Mehrdad G, Mayer JRR (2014) Validation of volumetric error compensation for a five-axis machine using surface mismatch producing tests and on-machine touch probing. 87:89-95
6. NAS979 (1969) Uniform cutting test-NAS series, metal cutting equipment. NAS, USA
7. ISO 10791-7 (1988) Test conditions for machining centres—part 7: accuracy of a finished test piece
8. Burak S, Yusuf A, Elizabeth C (2009) Modeling and control of contouring errors for five-axis machine tools—part I: modeling. J Manuf Sci Eng 131:1–8
9. Zhenya H, Jianzhong F, Liangchi Z, Xinhua Y (2015) A new error measurement method to identify all six error parameters of a rotational axis of a machine tool. Int J Mach Tools Manuf 88:1–8
10. Song ZY, Cui YW (2009) S-shape detection test piece and a detection method for detection the precision of the numerical control milling machine. United States, Invention Patent, US8061052B2
11. Yamaguchi F (1988) Curves and surfaces in computer aided geometric design. Springer
12. Zhang YM, Lin XL, Wang XD, Cai GQ (2004) The study on the dynamic characteristic of high speed machine tool and experiment validate. Mater Sci Forum: 471–472
13. Ratchev S, Govender E, Nikov S et al (2003) Force and deflection modeling in milling of low-rigidity complex parts. J Mater Process Technol 143–144:796–801